264 Transactions of the Korean Society of Mechanical Engineers, Vol. 8, No. 3, pp. 264~273, 1984.

<Original>

Initial Imperfection Sensitivity in Stiffened Plates

Chon Wook Kim* and Chong Jin Won**

(Received February 6, 1984)

補强板의 初期缺陷 敏感性 硏究

金 天 旭·元 鍾 鎭

抄 錄

初期缺陷이 있는 補强平板의 非線型 運動方程式을 Galerkin method에 의하여 유도하였다. Runge-Kutta method를 사용하여 step-load를 받고 있는 補强平板의 動的 挫屈問題의 數値解를 구하였다. 靜的 挫屈實驗에 의하여 挫屈荷重을 결정함에 있어 動的 解析法을 응용할 수 있음을 입증하였으며, step-load를 받는 補强平板의 動的 挫屈解析으로 靜的挫屈의 初期缺陷 敏感性을 解析하였다. 補强平板의 初期缺陷 敏感性은 平板보다 훨씬 낮으며 補强材의 偏心比가 높을수록 敏感性은 둔화된다.

1. Introduction

In general the plates which are used in various structural members are reinforced whith stiffeners. Increasingly the trend in steel structures has been to use thin-walled structures composed of assemblages of thin plates, such as box girder in cranes or bridges, oil rig platforms, etc., permitting efficient use of materials. However, as the designs are optimized from the stand-point of buckling, it is apparent that the mechanics of buckling behaviour of these structural forms becomes increasingly complicated.

The earliest solution of a buckling problem of flat plates was given by Bryan[1] in 1891. He applied the energy method to the analysis for a rectangular plate which is simply-supported on all its edges and acted upon two opposite sides by a uniformly distributed compressive load in the midplane of the plate. This energy method has been used in obtaining approximate solutions for stiffened plates by Timoshenko[2] in 1913.

The buckling theory of plates is one of the classical theories in solid mechanics. The main reason investigating the buckling phenomena of plates is the discrepancy between the theory and experiment. Generally, experimental buckling loads have been much lower than theoretical values. For many years, it has been speculated that these discrepancies might be attributed primarily to very small initial imperfections in plate geometry.

In the shell theory the discrepancy between the theory and the experiment can be minimized by testing almost accurate specimens. Tennyson[3,4] describes the construction and testing in axial compression of five accurately made cylindrical shells 8 to 10 in. in diameter. The fact that very high values of the buckling load were obtained when initial imperfections were carefully minimized confirms that the initial imperfection is the major reason for the reduction in critical load.

The initial imperfection sensitivity of the plate is

* Member, Department of Mechanical Engineering, Yonsei University
** Member, Department of Mechanics & Design, Kookmin University

generally less sensitive than the cylindrical shell. However, in the case of plates it is known that the residual stresses due to welding and the initial imperfection result in the reduction of buckling strength of the plates under compression[5,6,7]. The initial imperfection sensitivity of the stiffened plate can be expected less sensitive than the flat plate, since the stiffeners act as columns under compressive loads.

Ekstrom[8] analyzed the elastic buckling of a simply supported rectangular orthotropic plate, with initial imperfections, under a rapidly applied compressive load. He used the large deflection plate equations to study inertial effects in the postbuckling phase. In his study initial imperfections decrease the critical loads of the orthotropic plates.

In this paper the effect of initial imperfections is analyzed by the dynamic buckling mode. The stiffeners are located symmetrically to the plate and parralled to the compressive load. Experiment is also conducted to investigate the relation between the dynamic buckling mode and the static buckling. The initial imperfection sensitivity is analyzed by numerical solution of the nonlinear dynamic buckling equation.

2. Buckling Theory of Stiffened Plates

2.1. Governing Equations

Generally, the nonlinear equation of motion of the plate is based on the assumptions which are used in the Karman type theory. In deriving governing equations of stiffened plates, additional assumptions are established;

(1) Application of the large deflection plate theory is capable.
(2) In-plane inertia terms are lower order of importance compared to the normal inertia.
(3) The plate is symmetrically stiffened by equally spaced stiffeners.
(4) The entire plate including the stiffeners is activated in the buckling, that is, local buckling are not considered.
(5) The shear membrane force is carried entirely by the skin and the torsional rigidity of the stiffeners cross section are added to that of the plate.
(6) Plane stress condition is assumed before buckling The stiffeners have stiffness only in their plane. The stiffness of the stiffeners perpendicular to their plane is neglected.

Fig.1 shows the plate with the stiffened geometry and the coordinate system. Fig.2 shows the stress resultants and moments acting on the stiffened plate element.

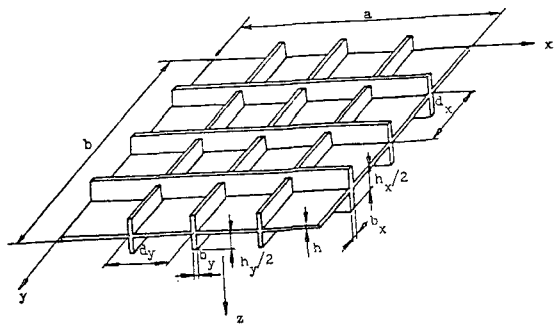

Fig. 1 Plate with symmetric stiffeners

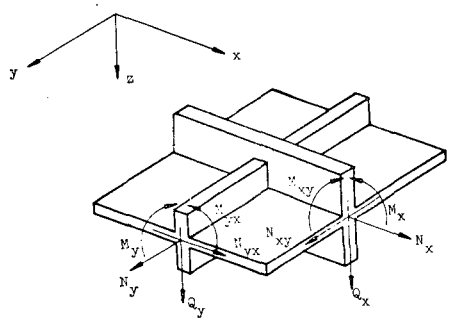

Fig. 2 Stress resultants and moments

Normal strains ε_x, ε_y and shear strain γ_{xy} in the stiffened plate can be represented as

$$\varepsilon_x=\varepsilon_x^0+z\kappa_x$$
$$\varepsilon_y=\varepsilon_y^0+z\kappa_y$$
$$\gamma_{xy}=\gamma^0_{xy}-2z\kappa_{xy} \quad (1)$$

where ε_x^0, ε_y^0, and γ^0_{xy} denote plane strains on the middle surface of the plate and $\kappa_x, \kappa_y, \kappa_{xy}$ denote the change of curvatures and twist.

Relations between stresses and strains can be represented as, for the plate

$$\sigma_x=\frac{E}{1-\nu^2}(\varepsilon_x+\nu\varepsilon_y)$$
$$\sigma_y=\frac{E}{1-\nu^2}(\varepsilon_y+\nu\varepsilon_x) \tag{2}$$
$$\tau_{xy}=\frac{E}{2(1+\nu)}\gamma_{xy}$$

where E and ν denote longitudinal elastic constant and Poisson's ratio, respectively,

and for stiffeners

$$\sigma_x'=E_x\varepsilon_x$$
$$\sigma_y'=E_y\varepsilon_y \tag{3}$$
$$\tau_{xy}'=0$$

where E_x and E_y denote longitudinal elastic constants of longitudinal and transverse stiffeners, respectively.

Using the resultant stresses and moments the constitutive equations for the stiffened plate can be written in the form

$$\begin{pmatrix}N_x\\N_y\\N_{xy}\\M_x\\M_y\\M_{xy}\end{pmatrix}=\begin{pmatrix}C_{11}&C_{12}&0&0&0&0\\C_{12}&C_{22}&0&0&0&0\\0&0&C_{33}&0&0&0\\0&0&0&C_{44}&C_{45}&0\\0&0&0&C_{45}&C_{55}&0\\0&0&0&0&0&C_{66}\end{pmatrix}\begin{pmatrix}\varepsilon_x\\\varepsilon_y\\\gamma_{xy}\\\kappa_x\\\kappa_y\\\kappa_{xy}\end{pmatrix} \tag{4}$$

where the stiffeness parameters are

$$C_{11}=C+\frac{E_xb_xh_x}{d_x} \qquad C_{12}=\nu C$$
$$C_{22}=C+\frac{E_yb_yh_y}{d_y} \qquad C_{33}=\frac{(1-\nu)C}{2}$$
$$C=\frac{Eh}{1-\nu^2} \qquad D=\frac{Eh^3}{12(1-\nu^2)} \tag{5}$$
$$C_{44}=D+\frac{E_xI_x}{d_x} \qquad C_{45}=\nu D$$
$$C_{55}=D+\frac{E_yI_y}{d_y}$$
$$C_{66}=(1-\nu)D+\frac{1}{2}\left(\frac{G_xJ_x}{d_x}+\frac{G_yJ_y}{d_y}\right)$$
$$I_x=\frac{b_x}{12}\left\{(h+h_x)^3-h^3\right\}$$
$$J_x=\frac{h_xb_x^3}{3}\left(1-\frac{384}{\pi^5h_x}\tanh\frac{\pi h_x}{4b_x}\right)\left(\text{for } b_x<\frac{h_x}{2}\right)$$
$$I_y=\frac{b_y}{12}\left\{(h+h_y)^3-h^3\right\}$$
$$J_y=\frac{h_yb_y^3}{3}\left(1-\frac{384}{\pi^5h_y}\tanh\frac{\pi h_y}{4b_y}\right)\left(\text{for } b_y<\frac{h_y}{2}\right)$$

In the above parameters J_x and J_y are torsional constants depending on the values of the aspect ratio of the longitudinal and transverse stiffeners cross section, respectively[9].

In order to investigate the effect of initial imperfections to the critical load for stiffened plates, we introduce the second-order strain-displacement relations

$$\varepsilon_x^0=u_{,x}+\frac{1}{2}w_{,x}^2-\frac{1}{2}(w_{0,x})^2$$
$$\varepsilon_y^0=v_{,y}+\frac{1}{2}w_{,y}^2-\frac{1}{2}(w_{0,y})^2 \tag{6}$$
$$\gamma^0_{xy}=u_{,y}+v_{,x}+w_{,x}w_{,y}-w_{0,x}w_{0,y}$$

where u and v denote the displacements in x and y directions, respectively. $w\ (x,y,t)$ is the total displacement normal to the middle surface and $w_0(x,y)$ is the initial displacement normal to the middle surface. The changes of curvature are represented as

$$\kappa_x=-\bar{w}_{,xx},\quad \kappa_y=-\bar{w}_{,yy},\quad \kappa_{xy}=\bar{w}_{,xy} \tag{7}$$

where

$$\bar{w}=w-w_0$$

The equation of motion in the direction normal to the middle plane yields in the form of resultant moments

$$M_{x,xx}-2M_{xy,xy}+M_{y,yy}+(N_xw_{,xx}+2N_{xy}w_{,xy}+N_yw_{,yy})=\rho hw_{,tt} \tag{8}$$

Neglecting tangential inertias, equilibrium equations in x and y directions are identically satisfied by introducing stress function $F(x,y,t)$ which is defined as

$$N_x=hF_{,yy},\quad N_y=hF_{,xx},\quad N_{xy}=-hF_{,xy} \tag{9}$$

Using Eqs. (1), (4), (6), (7), (8) and (9), the equation of motion can now be written as

$$C_{44}\bar{w}_{,xxxx}+2(C_{45}+C_{66})\bar{w}_{,xxyy}+C_{55}\bar{w}_{,yyyy}=h(F_{,yy}w_{,xx}-2F_{,xy}w_{,xy}+F_{,xx}w_{,yy}-\rho w_{,tt}) \tag{10}$$

The compatibility condition for the large deflection theory is given as

$$\varepsilon^0_{x,yy}+\varepsilon^0_{y,xx}-\gamma^0_{xy,xy}=(w_{,xy})^2-w_{,xx}w_{,yy}-(w_{0,xy})^2+w_{0,xx}w_{0,yy} \tag{11}$$

From Eqs. (4) and (9), Eq. (11) yields

$$\frac{h}{C_{11}C_{22}-C_{12}^2}\left\{C_{11}F_{,xxxx}+\left(\frac{C_{11}C_{22}-C_{12}^2}{C_{33}}\right)F_{,xxyy}+C_{22}F_{,yyyy}\right\}=(w_{,xy})^2-w_{,xx}w_{,yy}-(w_{0,xy})^2+w_{0,xx}w_{0,yy} \tag{12}$$

Then, Eqs. (10) and (12) are governing equations for the symmetrically stiffened plate.

2.2. Buckling Equation

In case that all the edges of the rectangular stiff-

ened plate are simply-supported and subject to the in-plane load in the x direction, boundary conditions are

$$w=w_0=w_{,xx}=w_{0,xx}=0 \quad \text{at } x=0 \text{ and } x=a$$
$$w=w_0=w_{,yy}=w_{0,yy}=0 \quad \text{at } y=0 \text{ and } y=b \tag{13}$$

The deflection function for the stiffened plate which satisfies Eq. (13) will be assumed to be a single mode.

$$w(x,y,t)=f(t)\sin\frac{m\pi x}{a}\sin\frac{n\pi y}{b} \tag{14}$$

where $f(t)$ is the time-varying amplitude of w and m and n are the integer numbers of half waves in the x and y directions, respectively.

In analyzing the effects of initial imperfections, the initial and final shapes are usually assumed to be of the same basic form. Thus, $w_0(x,y)$ is taken as

$$w_0(x,y)=f_0\sin\frac{m\pi x}{a}\sin\frac{n\pi y}{b} \tag{15}$$

where f_0 is the amplitude of the initial imperfection.

If there is no restraint in the y direction at edges $y=0$ and $y=b$, F must satisfy

at $x=0$ and $x=a$,

$$\frac{1}{bh}\int_0^b N_x dy=\frac{1}{b}\int_0^b F_{,yy}dy=-p$$

at $y=0$ and $y=b$, (16)

$$\frac{1}{ah}\int_0^a N_y dx=\frac{1}{a}\int_0^a F_{,xx}dx=0$$

where p is defined as the average value of the compressive stress in the x direction.

Substituting Eqs. (14) and (15) into the compatibility condition, Eq. (12), one obtains a differential equation relating the stress function to the assumed deflection function.

$$\frac{h}{C_{11}C_{22}-C_{12}^2}\left[C_{11}F_{,xxxx}+\left(\frac{C_{11}C_{22}-C_{12}^2}{C_{33}}-2C_{12}\right)F_{,xxyy}+C_{22}F_{,yyyy}\right]=\frac{1}{2}\frac{m^2n^2\pi^4}{a^2b^2}\times\left(\cos\frac{2m\pi x}{a}+\cos\frac{2n\pi y}{b}\right)(f^2-f_0^2) \tag{17}$$

A solution of Eq. (17) which satisfies the conditions given by Eq. (16) is

$$F(x,y,t)=\frac{C_{11}C_{22}-C_{12}^2}{32h}\left(\frac{a^2n^2}{b^2m^2}\cos\frac{2m\pi x}{a}+\frac{b^2m^2}{a^2n^2}\cos\frac{2n\pi y}{b}\right)(f^2-f_0^2)-\frac{1}{2}py^2 \tag{18}$$

Substituting Eqs. (14), (15) and (18) into Eq. (10), the equation of motion yields

$$\left\{\frac{d^2f}{dt^2}+\frac{\pi^4}{h\rho}\left[\frac{C_{44}m^4}{a^4}+\frac{2(C_{45}+C_{66})m^2n^2}{a^2b^2}+\frac{C_{55}n^4}{b^4}\right](f-f_0)-\frac{m^2n^2p}{\rho a^2}f-\frac{\pi^4(C_{11}C_{22}-C_{12}^2)}{8h\rho}\left(\frac{n^4}{C_{11}b^4}\cos\frac{2m\pi x}{a}+\frac{m^4}{C_{22}a^4}\cos\frac{2n\pi y}{b}\right)f(f^2-f_0^2)\right\}\times\sin\frac{m\pi x}{a}\sin\frac{n\pi y}{b}=0 \tag{19}$$

Applying Galerkin's method, we obtain a nonlinear equation of motion as follows:

$$\frac{d^2f}{dt^2}+\frac{\pi^4}{\rho h}\left[\frac{C_{44}m^4}{a^4}+\frac{2(C_{45}+C_{66})m^2n^2}{a^2b^2}+\frac{C_{55}n^4}{b^4}\right]\times(f-f_0)-\frac{m^2\pi^2p}{\rho a^2}f+\frac{(C_{11}C_{22}-C_{12}^2)\pi^4}{16\rho h}\left(\frac{m^4}{C_{22}a^4}+\frac{n^4}{C_{11}b^4}\right)\times f(f^2-f_0^2)=0 \tag{20}$$

where m and n are odd integer numbers.

Omitting d^2f/dt^2 and nonlinear terms and setting $f_0=0$, the static critical buckling load of the perfect stiffened plate can be obtained as

$$\frac{\pi^2}{h}\left[C_{44}\left(\frac{m}{a}\right)^4+2(C_{45}+C_{66})\left(\frac{m}{a}\right)^2\left(\frac{n}{b}\right)^2+C_{55}\left(\frac{n}{b}\right)^4\right]-\left(\frac{m}{a}\right)^2\frac{P}{bh}=0 \tag{21}$$

where $P=pbh$

From Eq. (21), with $n=1$, the static critical buckling load P_{cl} is given as

$$P_{cl}=\frac{\pi^2C_{44}}{b}\left[\left(\frac{mb}{a}\right)^2+\frac{2(C_{45}+C_{66})}{C_{44}}+\frac{C_{55}}{C_{44}}\left(\frac{a}{mb}\right)^2\right] \tag{22}$$

and the least critical load

$$(P_{cl})_{\min}=\frac{2\pi^2}{b}\left[(C_{44}C_{55})^{1/2}+C_{45}+C_{66}\right] \tag{23}$$

occurs when $(C_{55}/C_{44})^2(a/b)$ is an integer.

In order to generalize the solution of Eq. (20), the following nondimensional parameters are introduced

$$\zeta=\frac{f}{h},\quad \zeta_0=\frac{f_0}{h},\quad \beta=a/b$$
$$\tau=\frac{\pi^2t}{a^2}\sqrt{\frac{C_{44}}{\rho h}},\quad \Gamma=\frac{P}{P_{cl}}$$
$$R_1=\frac{C_{45}+C_{66}}{C_{44}},\quad R_2=\frac{C_{55}}{C_{44}},$$

$$R_3=\frac{(C_{11}C_{22}-C_{12}^2)h^2}{C_{22}C_{44}},\quad R_4=\frac{C_{22}}{C_{11}} \tag{24}$$

With these substitution, and for $n=1$, Eq. (20) becomes

$$\frac{d^2\zeta}{d\tau^2}+(m^4+2R_1m^2\beta^2+R_2\beta^4)(\zeta-\zeta_0)-(m^4+2R_1m^2\beta^2+R_2\beta^4)\Gamma\zeta+\frac{R_3}{16}(m^4+R_4\beta^4)(\zeta^2-\zeta_0^2)\zeta=0 \tag{25}$$

Since $R_1=R_2=R_4=1$ and $R_3=12(1-\nu^2)$ for the unstiffened plate, Eq. (25) becomes for isotropic plates

$$\frac{d^2\zeta}{d\tau^2}+(m^2+\beta^2)^2(\zeta-\zeta_0)-(m^2+\beta^2)^2\Gamma\zeta+\frac{3(1-\nu^2)}{4}(m^4+\beta^4)(\zeta^2-\zeta_0^2)\zeta=0 \tag{26}$$

3. Numerical Examples

The dynamic buckling load of the stiffened plate is limited to the step-load which is closely related to the static load, since the main purpose of this study is the investigation of the effect of initial imperfections.

As shown in Fig. 3, the loading condition in the present study is

$$\Gamma=0 \text{ at } \tau=0$$
$$\Gamma=\Gamma_0 \text{ at } \tau>0 \tag{27}$$

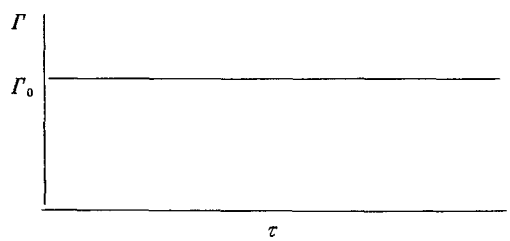

Fig. 3 Shape of loading

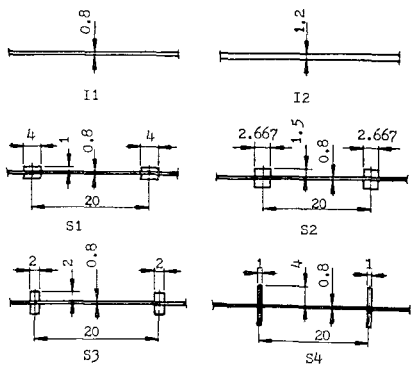

Fig. 4 Shapes and dimensions of the specimens for numerical examples

In order to investigate the effect of eccentricity of stiffeners, 4 kinds of stiffening types are selected as numerical examples and the dynamic buckling of isotropic plates is also analyzed. Properties of the plates in numerical examples are shown in Table 1 and the geometries of the plates are shown in Fig.4.

Eq. (25) is numerically solved by the fourth order Runge-Kutta method. Numerical results are given for the longitudinally stiffened plate with $\beta=1.25$ in order to compare with static buckling experiments. Initial deflections ζ_0 which are used in the numerical analysis are 0.0001 for perfect plates and 0.01, 0.05, 0.1, 0.2, 0.4, 0.6, 0.8 and 1.0 for the plates with initial deflections. Initial conditions of numerical integrations are $\zeta=\zeta_0$ and $d\zeta/d\tau=0$ at $\tau=0$.

When it is assumed that the mode type in the linear buckling analysis is pertinent to that in the nonlinear buckling analysis, the value of m which give the minimum critical buckling load is selected by the value which minimize the critical buckling load.

Table 1 Properties of the plates

Specimen	h (mm)	$A_x(b_xh_x)$ (mm²)	I_x (mm⁴)	J_x (mm⁴)	d_x (mm)	E (kg$f$/mm²)	E_x (kg$f$/mm²)	ν
S1	0.8	8(4×2)	7.147	2.248	20	7×10^3	7×10^3	0.33
S2	0.8	8(2.667×3)	12.082	4.5996	20	〃	〃	〃
S3	0.8	8(2×4)	18.347	7.598	20	〃	〃	〃
S4	0.8	8(1×8)	56.747	2.248	20	〃	〃	〃
I1	0.8	0	0	0	—	〃	〃	〃
I2	1.2	0	0	0	—	〃	〃	〃

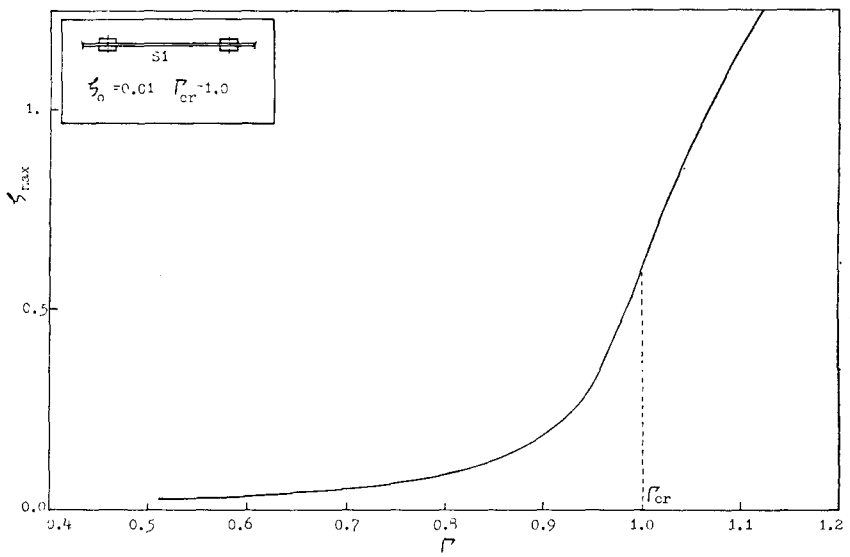

Fig. 5 Amplitude-load curve for a stiffened plate under step-load

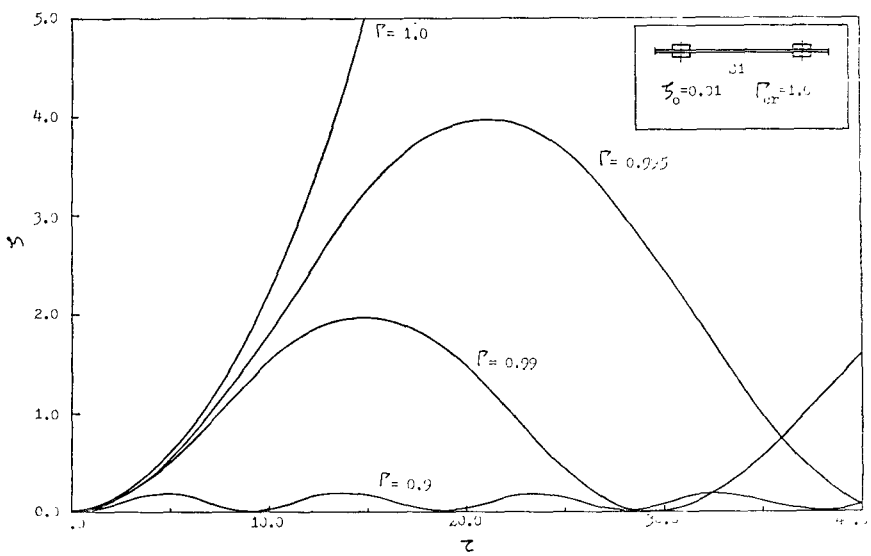

Fig. 6 Linear response curves of the stiffened plate under step-load

$(P_{cl})_{min}$, which is given as Eq. (23), exists only in the case that value of $(C_{55}/C_{44})^2$ (a/b) is an integer and it can not be generally applied. For β= 1.25, the value of m which gives $(P_{cl})_{min}$ in the buckling of stiffened plates and isotropic plates is 1.

Dynamic buckling loads are obtained from the amplitude-load curves which are plotted by the numerical results Fig. 5 shows a typical amplitude-load curve of a stiffened plate. From the nonlinear characteristics of the deflection of the plate, we can find an inflection point on the amplitude-load curve. The load corresponding to this inflection point is

defined as the dynamic buckling load P_{cr}.

In order to examine the propriety of this dynamic buckling load, only the linear terms in Eq. (25) are plotted as shown in Fig. 6. The amplitude of the linear response curve becomes infinite at the dynamic buckling load. This is the same concept as the Euler theory for the buckling of a column.

In Table 2, static buckling loads obtained by the linear theory (i.e., classical buckling theory), dynamic buckling loads, and nondimensionalized buckling loads of the stiffened and isotropic plates are shown.

Initial imperfections were taken as $\zeta_0=0.01$, 0.05, 0.1, 0.2, 0.4, 0.6, 0.8 and 1.0, and dynamic buckling loads for all kinds of specimens are shown in Table 3. Using these data the nondimensional buckling loads vs initial imperfections are plotted as shown in Fig. 7.

Table 2 Critical values of perfect stiffened and unstiffened plates under axial step-load

Specimen	ζ_0	P_{cl}(kg$f$)	P_{cr}(kg$f$)	Γ_{cr}
S1	0.0	271.84	273.2	1.005
S2	〃	388.21	390.15	1.005
S3	〃	536.09	538.77	1.005
S4	〃	1185.64	1191.57	1.005
I1	〃	115.85	116.43	1.005
I2	〃	390.98	392.93	1.005

Table 3 Critical values of imperfect stiffened and unstiffened plates under axial step-load

Specimen	ζ_0	P_{cr}(kg$f$)	Γ_{cr} (P_{cr}/P_{cl})
S1	0.10	265.04	0.975
	0.20	255.53	0.940
	0.40	229.7	0.845
	0.60	202.52	0.745
	0.80	173.98	0.640
	1.00	144.08	0.530
S2	0.10	382.39	0.985
	0.20	368.8	0.950
	0.40	341.62	0.880
	0.60	308.63	0.795
	0.80	269.81	0.695
	1.00	229.04	0.590
S3	0.10	530.73	0.990
	0.20	520.0	0.970
	0.40	490.52	0.915
	0.60	450.31	0.840
	0.80	412.79	0.770

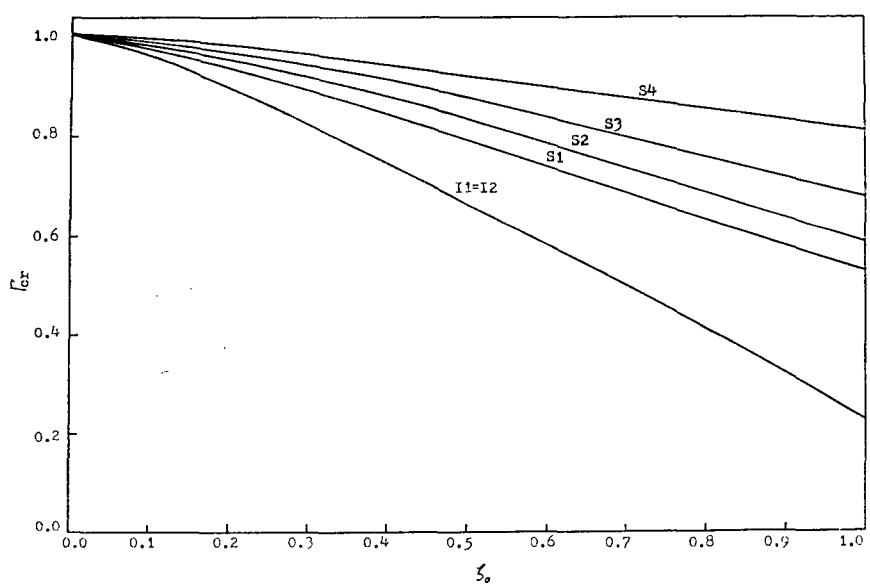

Fig. 7 Effect of initial imperfections to the dynamic buckling loads of stiffened and unstiffened plates under spep-load

	1.00	364.54	0.680
S4	0.10	1179.71	0.995
	0.20	1161.93	0.980
	0.40	1114.5	0.940
	0.60	1055.22	0.890
	0.80	1013.72	0.855
	1.00	966.3	0.815
I1	0.10	111.8	0.965
	0.20	104.27	0.900
	0.40	86.31	0.745
	0.60	68.35	0.590
	0.80	46.92	0.405
	1.00	27.22	0.235
I2	0.10	377.3	0.965
	0.20	351.88	0.900
	0.40	2191.88	0.745
	0.60	230.68	0.590
	0.80	158.35	0.405
	1.00	91.88	0.235

4. Experiments

4.1. Specimens

Specimens are made by aluminium plates(A1050P). Stiffeners are joined on the plate with a strong adhesive (Araldite). The elastic properties of the specimen are measured with the electric universal testing machine and the values of measurement are found as $E=7000\ kgf/mm^2$ and $\nu=0.33$.

Four kinds of specimens, I2, S1, S2 and S3 are selected for experiment among 6 kinds of specimens which are shown in Fig. 4.

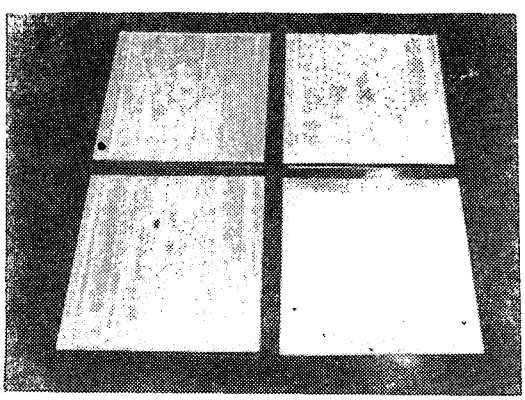

Fig. 8 Photo of stiffened and unstiffened plate specimens

In order to investigate the effects of initial imperfections on the buckling load, 4~6 kinds of initially imperfect specimens for each specimen are manufactured. In order to make initially imperfect specimens satisfy the initial deflection function as Eq. (15), the buckled specimens are used.

4.2. Experimental Apparatus and Experimental Procedure

As shown in Fig. 9, compressive loads are applied by the hydraulic universal testing machine (Shimadzu, RH-30) and measurements of compressive loads were carried out with a load cell, a dynamic strain amplifier (6ch.) and a recorder.

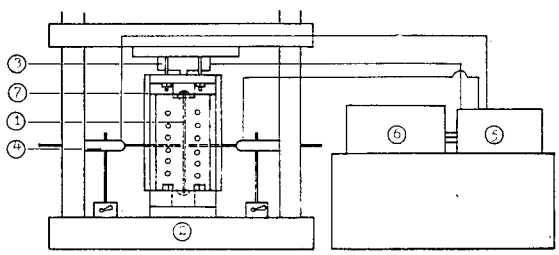

① Specimen
② U.T.M.
③ Load cell
④ Displacement transducer
⑤ Dynamic strain amplifier
⑥ Recorder
⑦ Simply-supported test-rig

Fig. 9 Schematic diagram of the experimental apparatus

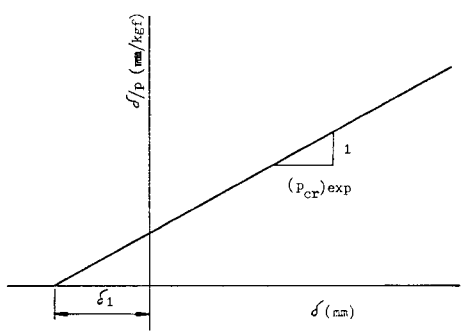

Fig. 10 Static buckling load

Applied loads and deflections of the center of the plate are recorded and calibrated to be converted into real values of loads and deflections. These loads and deflections are plotted by the Southwell method[10] and critical buckling loads are calculated. In Fig. 10 the Southwell method is shown and the straight line is obtained from plotting data by the least square method.

4.3. Experimental Results

In Fig. 11, an example of determination of the buckling load by the Southwell method is shown. Experimental results for the stiffened and isotropic plates are shown in Table 4.

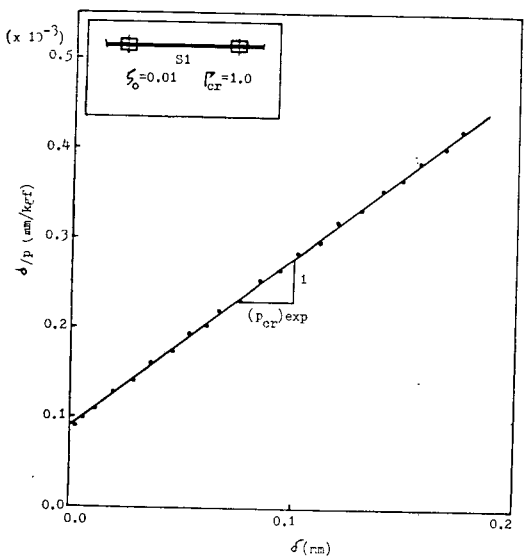

Fig. 11 Static buckling load of specimen

5. Discussion

5.1. Dynamic Bucking Load

It is difficult to study the initial imperfection for a real structure by the static analysis. Since the simulation by the computer is possible and the numerical analysis can be applied in the dynamic analysis, one can use the dynamic analysis to study the initial imperfection sensitivity of the stiffened plate.

As shown in Fig. 3, the dynamic load is instantaneously applied to the constant load Γ_0. The dynamic buckling load is a little larger than the static buckling load but is almost the same. Comparing the data in Table 2 and 4 with the specimen I2, the dynamic buckling load is larger than static buckling loads by 0.5%.

Table 4 Experimental results for the buckling loads of plates

Specimen	ζ_0	$(P_{cr})_{exp}$ (kg$f$)	$(P_{cr})_{th}$ (kg$f$)	$(\Gamma_{cr})_{exp}$
I 2	0.00	404.73	390.98	1.035
	0.13	374.56	〃	0.958
	0.22	350.66	〃	0.897
	0.26	336.55	〃	0.861
	0.36	300.51	〃	0.769
	0.50	246.83	〃	0.634
	0.90	105.39	〃	0.270
S1	0.00	273.94	271.84	1.008
	0.10	264.17	〃	0.972
	0.37	229.96	〃	0.846
	0.5	213.4	〃	0.785
	0.8	169.68	〃	0.624
S2	0.00	393.26	388.21	1.013
	0.10	382.39	〃	0.985
	0.20	369.58	〃	0.952
	0.25	362.59	〃	0.934
	0.39	341.24	〃	0.879
	0.54	315.61	〃	0.813
	0.93	237.97	〃	0.613
S3	0.00	546.28	536.09	1.019
	0.14	528.05	〃	0.985
	0.5	470.15	〃	0.877
	0.91	331.93	〃	0.706

5.2. Initial Imperfection Sensitivity

The initial imperfection sensitivity of the non-stiffened plate is relatively high. As shown in Table 3, when $\zeta_0=1$, $\Gamma_{cr}=0.235$ and this value is little more than that of the cylindrical shell[11]. But, in the case of S3, which is adequately stiffened, $\Gamma_{cr}=0.68$. In the case of S4, which has a large eccentricity in the stiffener, $\Gamma_{cr}=0.815$. Thus, one can conclude that the initial imperfection sensitivity becomes lower with increasing eccentricity in the stiffener.

Table 5 Buckling loads for perfect stiffened and unstiffened plates

Specimen	I 1	I 2	S 1	S 2	S 3	S 4
P_{cl}(kg f)	115.85	390.98	271.84	388.21	536.09	1185.64
$P_{cl}/(P_{cl})_{11}$	1.0	3.375	2.346	3.351	4.627	10.234
$\lambda=h_x/h$	0.0	0.0	2.5	3.75	5.0	10.0

5.3. Eccentricity of the Stiffener

In Table 5, values of the ratio of the buckling load of perfect stiffened plates and isotropic plates are shown.

In Table 5, the critical loads of the S1 and S2 are smaller than that of I2. However S3 and S4, which are same sectional area and larger eccentricities, show much larger critical loads. Thus, one can conclude that the effectiveness of the stiffener depends on the eccentricity ratio λ of stiffened plates.

6. Conclusion

The dynamic buckling analysis is employed to investigate the buckling strength of stiffened plates with various initial imperfections. The dynamic buckling load of a stiffened plate under step compressive stress shows almost same value of the classical buckling load of stiffened plates. This analogy is supported by the experimental results. The initial imperfection sensitivity of the stiffened plate is analyzed by the dynamic buckling analysis and static experiment. The initial imperfection sensitivity of the stiffened plate is less sensitive than the isotropic (unstiffened) plate. The eccentricity of the stiffener is the major factor for the sensitivity and the eccentricity ratio is inversely proportional to the initial imperfection sensitivity of stiffened plates.

Finally the authors wish to express their deep appreciation to the Korea Science and Engineering Foundation for supporting the research grant.

References

(1) Bryan, G.H., On the Stability of a Plane Plate under Thrusts in Its Own Plane, with Applications to the Buckling of the Sides of a Ship, Proc. London Math. Soc., Vol. 22, pp. 54～67, 1891

(2) Timoshenko, S.P. and Gere, J.M., Theory of Elastic Stability, McGraw-Hill Book Co., New York, N.Y., pp. 348～356, 1961

(3) Tennyson, R.C., "An Experimental Investigation of the Buckling of Circular Cylindrical Shells in Axial Compression Using the Photoelastic Technique, Rept. 102, Institute of Aerospace Science, University of Toronto. 1964

(4) Tennyson, R.C., "A Note on the Classical Buckling Load of Circular Cylindrical Shells under Axial Compression" AIAA Journal, Vol. 1, pp. 475～476, 1963

(5) 吉識 藤田 川井, "残留應力が板の挫屈强度におよぼす影響", 日本造船協會論文集, 第107號, pp. 187～194, 1960

(6) Ueda, Y. and Tall, L., "Inelastic Buckling of Plates with Residual Stresses"., Publications, IABSE, Zurich, pp. 211～254, 1967

(7) 山本善一, "初期たわみを有する柱と板の塑性變形を伴ラ挫屈", 日本造艦協會論文集, 第97號 pp. 57～58, 1955

(8) Ekstrom, R.E., "Dynamic Buckling of a Rectangular Orthotropic Plate", AIAA Journal, Vol. 11, pp. 1655～1659, 1973

(9) J.T. Oden, "Mechanics of Elastic Structures", McGRAW-HILL Book co. p. 44, 1967

(10) R.V. Southwell, Proc. Roy. Soc., Lond. A135, p. 601, 1932

(11) Kim, C.W. and Lu, S.Y., "Dynamic Stability of Orthotropic Cylindrical Shells under Axial Compression", Trans. of KSME, Vol. 7, No. 1, pp. 73～82, 1983